Improving Automated Pacing at the End of the Effective Refractory Period

Pascal Maierhofer[1], Jule Bender[1], Patrick M. Boyle[2], Edward Vigmond[3], Axel Loewe[1]

[1]Institute of Biomedical Engineering, Karlsruhe Institute of Technology (KIT), Karlsruhe, Germany
[2]Department of Bioengineering, University of Washington, Seattle, WA, USA
[3]Liryc Heart Rhythm Disease Institute, Fondation Bordeaux University, Bordeaux, France

Abstract

Atrial fibrillation (AF) vulnerability is one of the key metrics used in in silico studies to assess arrhythmia mechanisms and to evaluate personalized ablation strategies. The pacing at the end of the effective refractory period (PEERP) protocol by Azzolin et al. is commonly used to predict in silico vulnerability to reentry initiation. However, identification of the ERP can fail in models with patchy fibrotic regions. This work introduces a new method to find the ERP based on local activation times (LATs). This new method, combined with further improvements and refactoring applied to PEERP, is compared against the old version based on one tissue patch and 22 patient-specific bi-atrial models. Using the tissue patch example, we describe how PEERP can fail in fibrotic border regions at detecting the correct ERP. The 22 personalized models comprised a total of 1136 stimulation points. While the old PEERP protocol induced 438 reentries, the new protocol found 110 more inducing points (548). This improved implementation provides a well-defined induction method suitable for comparing AF inducibility.

1. Introduction

Atrial fibrilation (AF) is the most common sustained arrhythmia worldwide with an ever-increasing prevalence [1]. Comparing different AF treatment strategies in silico calls for a standardized protocol to compare AF vulnerability. To tackle this problem, Azzolin et al. [2] developed the pacing at the end of the effective refractory period (PEERP) protocol. The effective refractory period (ERP) is defined as the shortest period between two stimuli applied at one point which elicits two activations. As multiple studies [3–6] used this approach, PEERP has become one of the standard tools for AF initiation. While the detection of the effective refractory period (ERP) is crucial for the PEERP algorithm, it currently only checks for voltage thresholds being exceeded around the stimulation point. This voltage-based refractoriness detection, however, fails at fibrotic border regions, which we demonstrate in a tissue patch example in this work. To overcome this problem, we improved the original ERP detection to be resilient against complex activation patterns by focusing on the local activation times (LATs) with and without the added stimulus. Additionally, we describe the complete PEERP algorithm in detail and published a cleaned-up and well-documented version for the openCARP [7] framework.

2. Methods

2.1. Original PEERP

The original PEERP algorithm as introduced by Azzolin et al. [2] is based on a binary search to find the ERP. Before determining the ERP, pre-pacing is performed from the sinus node for five S1 beats. After this, all additional stimuli are placed at stimulation points in the atria. The initial guess for the ERP is the action potential duration at 94% repolarization. The end of the ERP is defined as the first captured stimulus, defined as the transmembrane potential exceeding $-50\,\mathrm{mV}$ in at least one point in a detection ring of 4-6 mm around the stimulation point. For each stimulation point, the search is stopped after 4 beats or if reentry is initiated. Reentry is defined by an activation in the detection ring between 900 and $1000\,\mathrm{ms}$ after the last stimulus. Based on the published PEERP code in the carputils repository (openCARP version 18.1 [8]), the further steps are as follows: Each ERP binary search starts with a search window defined by a lower bound and upper bound. While the initial S2 stimulus time is defined by the action potential duration (APD) after the last activation, the left bound is defined as $40\,\mathrm{ms}$ before the stimulus and the right bound as $APD/4$ after the stimulus. If the stimulus ($\mathrm{S_n}$) did not induce reentry, the lower bound of the search window for the next stimulus ($\mathrm{lb_{n+1}}$) is set to the next available stored checkpoint ($\mathrm{checkpoints} \in \{\mathrm{S2} + \{100, 200, 300\}\,\mathrm{ms}\}$) after the last activation (transmembrane voltage $\geq -50\,\mathrm{mV}$ in one point in the detection ring) at the stimulation point that is at least $60\,\mathrm{ms}$ after $\mathrm{S_n}$. Starting from this initial lower bound, the next $\mathrm{S_{n+1}}$ stimulus attempt is set as $\mathrm{lb_{n+1}} + 80\,\mathrm{ms}$ and

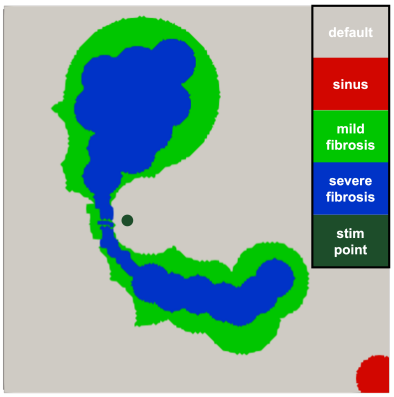

Figure 1. Test tissue patch for PEERP evaluation. Default atrial tissue (grey), mock sinus node for S1 initialization (red), fibrosis-based remodeling (green), non-conductive fibrosis (blue), stimulation point (dark green).

the upper bound is defined as $\mathrm{S}_{n+1} + 40\,\mathrm{ms}$.

2.2. Test Setup

The monodomain equation was solved with the openCARP [7] simulator. Cellular properties were modeled based on the Courtemanche et al. [9] model and modified per anatomical region based on Krueger et al. [10]. The default tissue conductivity was tuned to a longitudinal conduction velocity of $0.7\,\mathrm{m/s}$.

To test stability and identify potential for improvement of PEERP, we used two different test scenarios.

2.2.1. Tissue Patch

For testing and algorithmic improvements, we used a $2.5 \times 2.5\,\mathrm{cm}$ tissue surface patch with 4 different regions (see Figure 1). In the right lower corner of the patch, a mock sinus node, from which the sinus beat starts, was defined. While cellular and tissue properties were not changed in the default region, two different kinds of fibrotic remodeling (mild and severe fibrosis) were introduced yielding slow and non-conducting regions [11]. The selected stimulated node was placed close to the fibrotic patch, such that the detection ring in PEERP stretches to the other side of the fibrotic region. This setup simplifies full atrial electrophysiological simulations in the border regions between fibrotic and non fibrotic tissue.

2.2.2. Bi-Atrial Simulations

For evaluating the performance of the improved PEERP algorithm, 22 bi-atrial bilayer geometries were used. The properties of these geometries are detailed in [12]. Fibers and anatomical regions were annotated with AugmentA [13]. Mean inducibility was reported as 20.2% with a maximum number of four tested beats as suggested in the original PEERP formulation [2]. For this study, the same dataset was used; however, conductivities were tuned separately for all geometries to account for small changes in mesh resolution. Stimulation points were distributed equidistantly on the atria (distance of $2\,\mathrm{cm}$).

In addition to this cohort-based evaluation, one geometry (3% fibrotic tissue) was randomly selected to evaluate the influence of the maximum number of beats, which was increased to ten and the number of beats needed for induction per stimulation point was evaluated.

2.3. PEERP 2.0

The main change to the original PEERP algorithm is the detection of activation for the ERP search. In the original implementation, propagation was defined as a transmembrane voltage higher than $-50\,\mathrm{mV}$ in at least one point in a ring around the stimulation point. However, if two stimuli, e.g., the starting S1 beat from the sinus node and the first S2 stimulus from the stimulation point, are temporally close to each other, the first stimulus can exceed this $-50\,\mathrm{mV}$ threshold in the detection ring without the S2 stimulus propagating at all. To investigate this problem on a simplified scale, the tissue patch described in section 2.2.1 was used. If in this patch (Figure 1), the S2 point is stimulated with PEERP, the propagating wave travels around the fibrotic area, while PEERP already tries to set the next stimulus. This can lead to the binary search diverging to the lower bound of the search window, as every checked stimulus is misclassified as propagating, ultimately reducing PEERP to a periodic stimulation protocol.

To avoid this issue, we introduce LAT-based filtering, improving the ring-based detection. LATs give reliable information about propagation, while having a reduced dimensionality compared to a voltage time series. We therefore use LATs measured (first peak above $-50\,\mathrm{mV}$) in two different scenarios: First, the LATs without the new stimulus, and second, with the new stimulus. Using these two measurements, we can evaluate if an activation in the detection ring originates from the new stimulus or if this activation is already present in the ring before. Successful activation is thus defined by the difference $LAT_{\mathrm{new}} - LAT_{\mathrm{old}}$ being greater than $10\,\mathrm{ms}$. This $10\,\mathrm{ms}$ threshold is set to only detect substantial activation pattern changes. Therefore, a 3D-point x on the mesh is used for the activity detection if all the following three conditions are fulfilled:

$$\text{(i) } 2\hat{s} \;\leq\; \|\mathrm{x} - \mathrm{x}_{\mathrm{stim}}\| \;\leq\; 3\hat{s},$$

$$\text{(ii) } \mathrm{t}_{\mathrm{stim}} \;<\; \mathrm{LAT}_{\mathrm{new}}(\mathrm{x}) \;<\; \mathrm{t}_{\mathrm{max}},$$

$$\text{(iii) } \mathrm{LAT}_{\mathrm{new}}(\mathrm{x}) \;-\; \mathrm{LAT}_{\mathrm{old}}(\mathrm{x}) \;>\; 10\,\mathrm{ms},$$

with stimulus size $\hat{s}$, stimulus point $\mathrm{x}_{\mathrm{stim}}$, stimulus starting

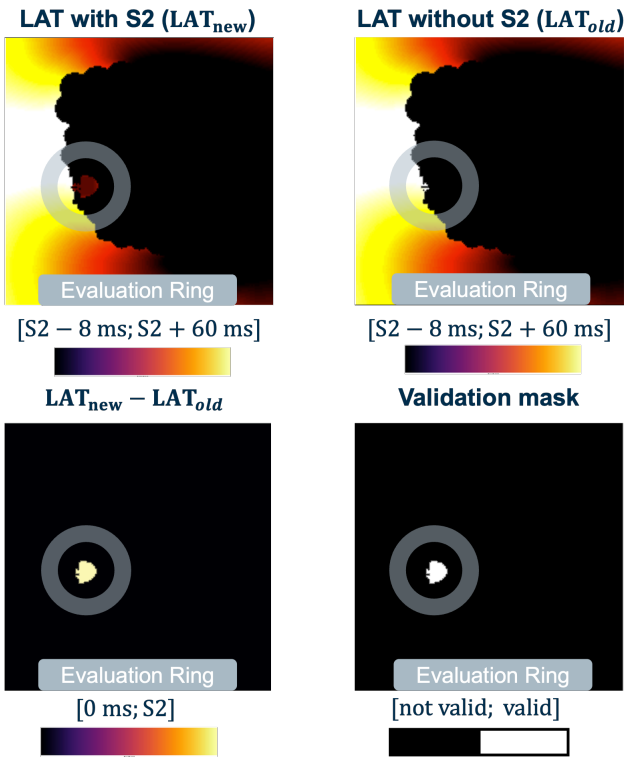

Figure 2. Process of activity detection of the new PEERP version. The LATs difference is calculated between the LATs with and without the new S2 stimulus. Valid points are then identified based on the LATs difference being greater than 10 ms.

time t_{stim} and end of simulation t_{max}. Successful propagation is then defined by one of the remaining valid x points having a transmembrane voltage greater than -50 mV.

As PEERP evaluates reentry inducibility using longer simulation runs after the last stimulus, we can use these simulations to generate the LAT without the new stimulus, thus not increasing execution time compared to the old PEERP version. An example of how this validation mask is created is shown in Figure 2.

3. Results

3.1. Tissue Patch

For the old PEERP algorithm, the search for the end of the ERP diverged for beats one, two, and three to the left boundary of the search window (see Figure 3). This happened because there was still activation opposite to the fibrotic region in the detection ring, and therefore the algorithm defined all stimuli as capturing/non-refractory, thus the ERP search was diverging to the lower bound of the ERP search window (example of a wrong detection in Figure 4). For the new PEERP version, the results of the ERP search were all more in the center of the initial search window compared to the old PEERP version (Figure 3). In addition, these four beats resulted in a re-entrant activity around the fibrotic region, whereas for the old stimulation sequence, no reentrant activation was observed.

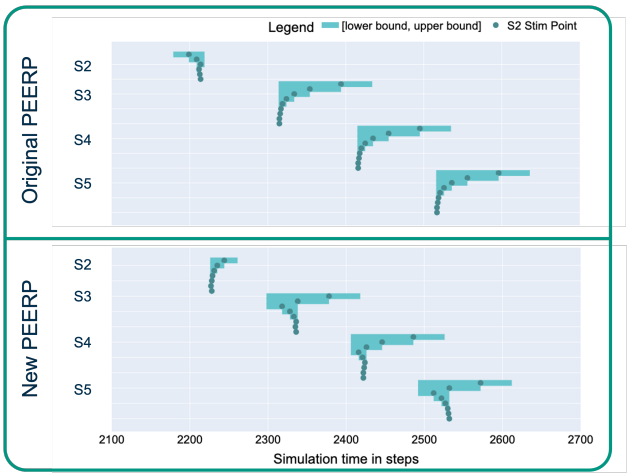

Figure 3. Convergence of the ERP search for four beats of the old (top) and new (bottom) PEERP version. Progress from top to bottom for the four stimuli (S2, S3, S4, S5). The dark green dots correspond to the tested S2 stimulus times, while the light green bars show the active search window for the ERP.

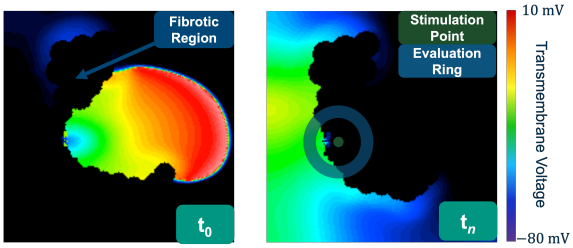

Figure 4. Example of wrong classification of refractoriness based on transmembrane voltage in the 2D tissue patch. The second stimulus (shortly before t_n) was placed in the refractory tissue; no activation can be seen around this point (t_n). However, the electrical wave elicited by S1 (before t_0) stimulus was still in the detection ring, resulting in PEERP classifying this stimulus as propagating.

3.2. Bi-Atrial Simulations

With the improved PEERP protocol, 548 stimulation points out of 1136 induced reentry episodes, while with the old PEERP version, only 438 points did. Additional reentries introduced by the updated PEERP were evenly distributed across models, with a mean of 5.2 ± 4.2 new

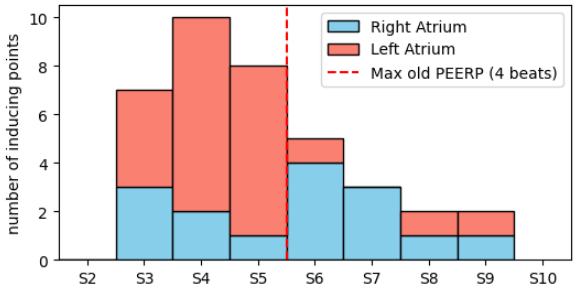

Figure 5. Number of reentry inducing stimulation points ordered by the first beat that induced the reentry

reentries per patient. Only one model exhibited one fewer reentry compared to its previous configuration.

When assessing the number of applied stimuli at 52 stimulation points (28 LA / 24 RA), most inducing points (25/38) were covered by the current limit of four beats (see Figure 5). However, 13 stimulation points only induced after applying more than 4 beats. Especially for the right atrial stimulation points, increasing the maximum number of beats increased the vulnerability (from 24% to 66%).

4. Discussion

With this work, we advanced the original PEERP algorithm by improving the ERP detection. This change, combined with small bug fixes (fully described in the carputils documentation[1]), leads to a higher inducibility not only in our test tissue patch but also for a study with 22 patient models and around 1000 stimulation points. The results for one mesh simulation suggest increasing the maximum number of applied beats to increase inducibility. However, confirmation on a larger cohort is needed.

This work, in combination with the carputils code documentation[1], describes the inner workings of the PEERP in silico protocol in detail. In addition, major refactoring of the original source code was done to improve maintainability, comparability, and comprehension of this algorithm, following the FAIR and CURE principles for research software development [14, 15]. All these changes are accessible in the revised PEERP implementation in carputils shipped with openCARP [8]. Collectively, these modifications improve the PEERP protocol as a well-defined tool for comparing AF inducibility.

Acknowledgments

Funded by the Deutsche Forschungsgemeinschaft (DFG, German Research Foundation) – Project number 394433254 and 529821741. The authors acknowledge support by the state of Baden-Württemberg through bwHPC.

[1] opencarp.org/documentation/carputils-documentation#master/md_doxygen_doc_related_pages_PEERP_documentation.html

References

[1] Van Gelder IC, et al. 2024 ESC Guidelines for the management of atrial fibrillation. Eur Heart J 2024;45(36):3314.

[2] Azzolin L, et al. A reproducible protocol to assess arrhythmia vulnerability. Front Physiol 2021;12:656411.

[3] Barrios Espinosa C, et al. A cyclical fast iterative method for simulating reentries in cardiac electrophysiology using an eikonal-based model. Engineering with Computers January 2025;41(4):2335–2358.

[4] Martínez Díaz P, et al. The right atrium affects in silico arrhythmia vulnerability in both atria. Heart Rhythm 1 2024; 21(6):799–805.

[5] Romitti GS, et al. Implementation of a Cellular Automaton for efficient simulations of atrial arrhythmias. Medical Image Analysis April 2025;101:103484.

[6] Banduc T, et al. Simulation-free prediction of atrial fibrillation inducibility with the fibrotic kernel signature. Medical Image Analysis October 2025;99:103375.

[7] Plank G, et al. The openCARP simulation environment for cardiac electrophysiology. Comput Meth Progr Biomed 6 2021;208:106223.

[8] openCARP consortium, et al. opencarp (v18.1), 2025. URL doi.org/10.35097/jynwqwhfftap7cvv.

[9] Courtemanche M, et al. Ionic mechanisms underlying human atrial action potential properties: insights from a mathematical model. Am J Physiol Heart Circ Physiol 1998; 275(1):H301–H321.

[10] Krueger MW, et al. Personalization of atrial anatomy and electrophysiology as a basis for clinical modeling of radiofrequency ablation of atrial fibrillation. IEEE Trans Med Imaging 1 2013;32(1):73–84.

[11] Roney CH, et al. Modelling methodology of atrial fibrosis affects rotor dynamics and electrograms. Europace 12 2016;18(suppl 4):iv146–iv155.

[12] Dıaz PM, et al. Insights from explainable machine learning on biatrial arrhythmia vulnerability assessment. In 2024 Computing in Cardiology Conference, volume 52. 2024; .

[13] Azzolin L, et al. AugmentA: Patient-specific augmented atrial model generation tool. Comput Med Imaging Graph 9 2023;108:102265–102265.

[14] Chue Hong NP, et al. FAIR principles for research software (FAIR4RS principles), May 2022. URL https://doi.org/10.15497/RDA00068.

[15] Sauro HM, et al. From FAIR to CURE: guidelines for computational models of biological systems. npj Systems Biology and Applications March 2026;ISSN 2056-7189.

Address for correspondence:

Pascal Maierhofer, Institute of Biomedical Engineering
Karlsruhe Institute of Technology (KIT)
publications@ibt.kit.edu